Numerical study on Multiple Independent Gate Field Effect Transistor

Han-geon Kim, Joong-sik Kim, Young-kyu Kim and Taeyoung Won

Department of Electrical Engineering, Inha University, 253 Yonghyun-dong,
Nam-ku, Incheon, Korea 420-751
Tel: +82-32-875-7436; Fax: +82-32-862-1350;
Email: khg@hsel.inha.ac.kr

ABSTRACT

In this paper, we present our numerical study on multiple independent gate field effect transistors (MIGFETs). Our theoretical work is based on 2-D quantum-mechanical simulation wherein a self-consistent the solution of Poisson-Schrödinger equation. This paper will review some of the advantages of MIGFET, device structure and optimization. Our numerical simulation revealed that L_{eff} / T_{eff} are required to be greater than 1.3 in order to maintain $V_T \leq 0.35V$ which is related to DIBL.

Keywords: MIGFET, Short Channel Effect, Quantum Mechanical

INTRODUCTION

As critical device features begin to approach 100nm, there are certain impediments like short channel effects (SCE), oxide and silicon tunneling, difficulty in lithographic patterning, etc [1]. Double-gate (DG) MOSFET structures can overcome these limitations to transistor scaling [1]. These devices offer excellent characteristics for a given bias across the gate. Independent gate electrodes on either side of these channels however enable the channel to be separately biased. [2]

The MIGFET devices comprise of gate on two side of the silicon fin. The gates in a MIGFET can independently control channel region. Planar Double devices have been demonstrated to offer independent double gate operation. The MIGFET demonstrates dynamic modulation of sub-threshold swing and threshold voltage by biasing the second gate. The shared fully depleted channel and perfectly matched independent gates has been advantageously. [3]

In this study, we performed a two-dimensional quantum mechanical simulation and investigated threshold voltage as well as I-V characteristics for MIGFET.

NUMERICAL MODEL

Our two-dimensional (2-D) QM model for obtaining the band structure is based on a self-consistent solution of coupled Poisson-Schrödinger equations in a simultaneous manner [4].

$$\nabla [\varepsilon (x, y) \nabla \Phi (x, y)] = -\rho (x, y) \qquad (1)$$

$$-\frac{\hbar^2}{2m^*}\frac{\partial^2 \Psi_n(x,y)}{\partial y^2} + V(x,y)\Psi_n(x,y) = E_n \Psi_n(x,y) \qquad (2)$$

where $\Psi_n(x,y)$ is the wave function of the nth eigenstates, $\hbar$ Planck's constant divided by 2π, m^* the effective mass, E_n the energy of the nth eigenstates, and V the potential energy given by $V = \Delta E_c(y) - q\Phi(x,y)$. Here, $\Delta E_c(y)$ is the band offset in the conduction band.

The mixed Dirichlet and von Neumann boundary conditions were used for the Schrödinger equation because the Dirichlet boundary conditions force density to decrease to zero at contacts while density increases under the von Neumann boundary conditions. For these reasons, we solved the Schrödinger equation under Dirichlet and von Neumann boundary conditions and normalized the states to 1/2.

$$\int |\Psi (z)|^2 dz = 1/2 \qquad (3)$$

This means that we obtain a constant function by summing the cosine functions from Dirichlet boundary conditions and the sine functions from von Neumann boundary conditions with normalization to 1/2.

By solving the Schrödinger equation, we obtain quantized states that are occupied by local quasi-Fermi levels. The two-dimensional quantum electron density n(x, y) is found using [5]

NSTI-Nanotech 2007, www.nsti.org, ISBN 1420061828 Vol. 1, 2007

$$n(x,y) = \sum_j n_j \left|\Psi_j(x,y)\right|^2 \qquad (4)$$

where n_j stands for the occupancy level of the j^{th} energy eigenstates. It is defined as

$$n_j = \frac{1}{\pi\hbar}\sqrt{2m^* k_B T}\, F_{-1/2}\left(\frac{E_F - E_j}{k_B T}\right) \qquad (5)$$

where $\Psi_j(x,y)$ is the wave function of the j^{th} eigenstates, E_F the Fermi level, E_j the energy of the j^{th} eigenstates, and F_k the Fermi-Dirac integrals of order k. These integrals are defined as

$$F_k(\eta) = \frac{1}{\Gamma(k+1)}\int_0^\infty \frac{u^k\, du}{e^{u-\eta}+1} \qquad (6)$$

We obtain the semi-classical current solution from the 1st moment of the Boltzmann equation by adopting a simple drift-diffusion model for electron current. The continuity equation for current density is

$$\nabla \cdot J_n(x,y) = -R(x,y) \qquad (7)$$

In order to obtain quantum mechanical solutions, we have employed an iterative procedure [4]. We start out by calculating the electric potential. Next, the program calculates a charge distribution using an iteration scheme. Thereafter, the program determines self-consistent solutions of Poisson and Schrödinger and current equations. The Newton's method has been employed with a constraint that should satisfy error criteria as outlined in [6].

SIMULATION RESULT

Figure 1 shows a top view of the cross section of the MIGFET used in this work. We employed a finite difference method for numerical analysis. As a test vehicle for verifying the validity of our numerical simulator, we choose N-channel MIGFET showing a relatively good short-channel performance down to a gate length of 20nm.

A couple of symmetric metal gates, the work function of which is Φ_M = 4.05 eV, are located on both sides of the channel. The source/drain region contact to metal is assumed to be ohmic with doping concentration of $1x10^{20}cm^{-3,}$ and the channel region is assumed to be intrinsic. The gate length (L_g) varies from 20 to 80nm and fin thickness (T_{fin}) varies from 10 to 30nm, while oxide thickness are fixed at 2nm.

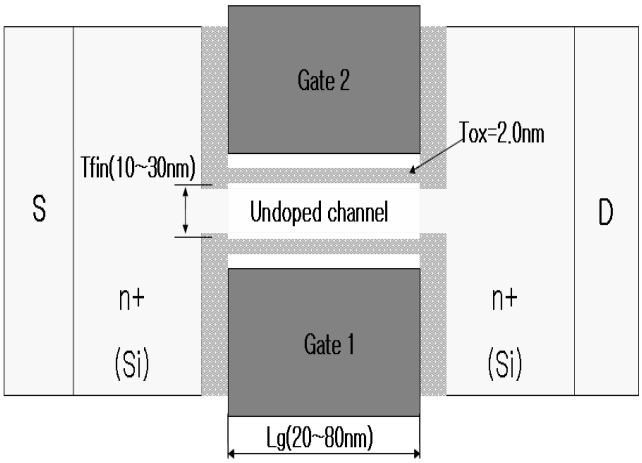

Fig. 1 Schematic diagram illustrating the MIGFET structure employed in this work.

Figure 2 shows the I_d-V_{gs} characteristics of the NMOS MIGFET in this work with L_g=80 and T_{fin}=30nm when V_{ds} = 0.1V, Vgs1 = 0.8V is applied. From the experimental data [3], we found that the sub-threshold slope (SS) is 87mV/dec and a linear V_T is 0.3V. Furthermore, the (SS) of our simulation is measured to be 74mV/dec and a linear V_T is 0.35V at the same V_{gs1}, V_{gs2}. Here, we can observe a little discrepancy between experimental data and the simulation, which seem to be due to the mismatch of the channel doping concentration of the real devices. Independently biasing the gates of the device the threshold voltage (V_T) and sub-threshold swing (SS) are modulation. In this figure, as V_{gs2} decreases, the devices show good drive and short channel characteristics. From the different point of view, we can observe that the MIGFET exhibit strengthened short channel control and sub-threshold behavior due to relatively a large ratio between the V_{gs1} and V_{gs2}.

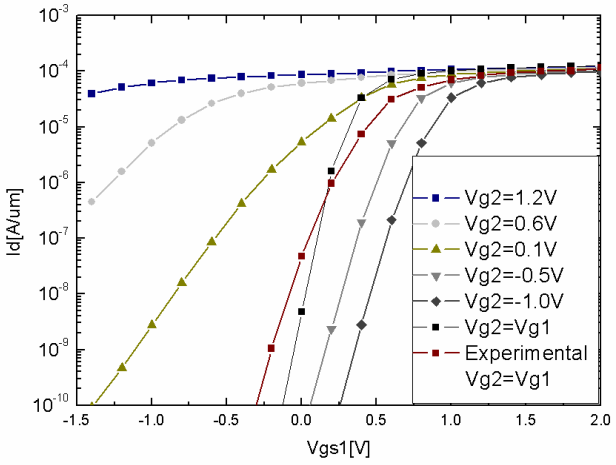

Fig. 2 Plot show I_d - V_g characteristics for MIGFET at Vgs2 of -1.0V to 1.2V and Vgs1 = 0.8V

In Fig. 3, is shown the output characteristics (I_d-V_d curves) for the MIGFET. The gate length is fixed at 100nm and drain voltage is swept to 1.5V while the gate voltage is increase with step of 0.25V. Referring to Fig. 3, we can see that sub-threshold current is well suppressed despite the intrinsic channel doping of the MIGFET structure.

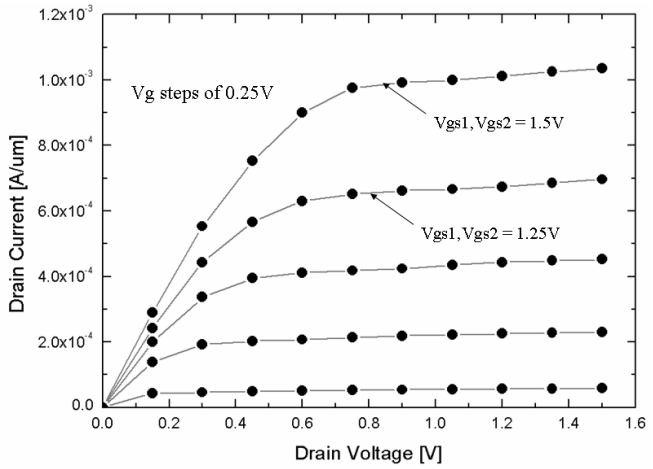

Fig. 3 Plot showing I_d - V_{gs} characteristics for Isolated n+/p+ strapped FinFET at L_g = 80nm, T_{fin} = 20nm.

Figure 4 shows the functional dependence of trans-conductance (Gm) at V_{ds} = 0.1V, V_{gs1} =0.8V on variation of V_{gs2}. The simulation reveals that Gm increase as V_{gs2} decrease. The gain (Gm) sensitivity to second gate bias demonstrates that this device is extremely useful for certain applications where the gain sensitivity to second gate bias can be advantageously.

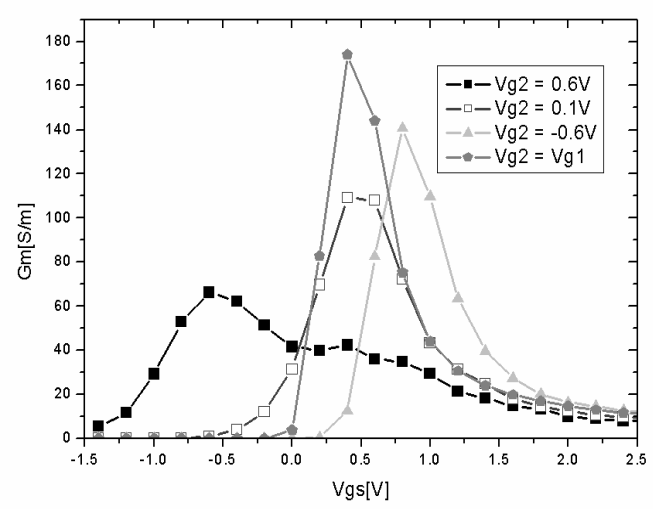

Fig. 4 Plot showing the dependence of transconductance (Gm) on Gate voltage at Gm.max = 178S/m at Vgs2 = Vgs1 = 0.8V.

Figure 5 shows the electron density profile change with second gate bias: (a) V_{gs1} = -0.8V (b) V_{gs1} = 0.0V (c) V_{gs1} = 0.8V, which are performed under condition V_{gs2} = 0.1V V_d = 0.1V. Electron density is observed under strong gate bias. The gate-1 influence on the conduction also diminishes for large bias once strong inversion at the gate-1 channel is attained due to inversion charge screening.

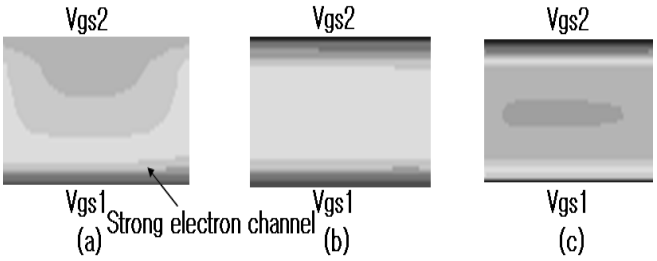

Fig. 5 Plot showing the carrier density profile change with second gate bias

To analyze SCE, we extract some parameters such as drain-induced barrier lowering (DIBL), V_T roll-off for N-channel MIGFET as a function of L_{eff}/ T_{eff} in comparison with published results. In this work, we performed numerical simulations under condition of L_g varying from 20 nm to 80 nm and T_{fin} varying from 10 nm to 30 nm. As we seen from Fig 6, we should choose a L_{eff}/ T_{eff} larger than 1.3 to maintain $V_t \leq 0.25$V which is related to DIBL. The strength of DIBL is measured from the difference in V_T as drain voltage change from 0.1V to 0.05V. It shows good short-channel behavior despite the fact that strong DIBL usually indicates poor short-channel behavior [7].

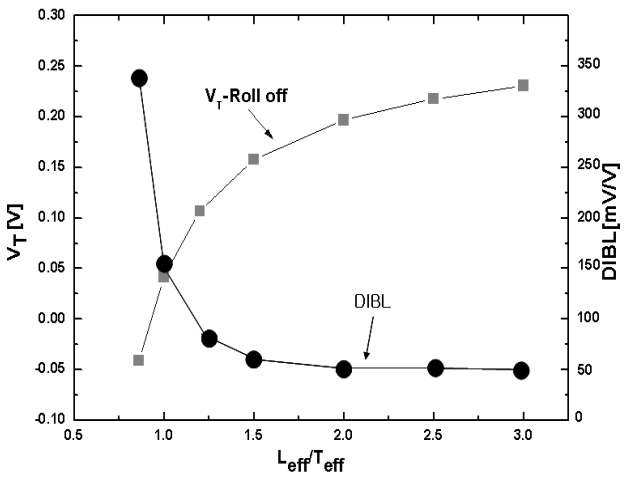

Fig. 6 V_T Roll-off and DIBL characteristics of MIGFET as a function L_{eff} / T_{eff}

NSTI-Nanotech 2007, www.nsti.org, ISBN 1420061828 Vol. 1, 2007

SUMMARY

A MIGFET is modeled and self-consistently using two-dimensional Poisson-Schrödinger for the quantum mechanical simulation. Our numerical simulation revealed that the threshold voltage (V_T) is controlled wide length of voltage by the variation of biasing the second gate. We also confirmed that that MIGFET demonstrates dynamic modulation of sub-threshold swing by biasing the second gate. And Short channel effects are appreciably suppressed for MIGFET in terms of DIBL, voltage roll-off. As CMOS scale down to low threshold voltage will be necessary, making V_T variation specifications more stringent. The device performance can overcome some of this limitation and V_T values have been demonstrated.

ACKNOWLEDGMENT

This research was supported by the MIC (Ministry of Information and Communication), Korea, under the ITRC (Information Technology Research Center) support program supervised by the IITA (Institute of Information Technology Advancement)" (IITA-2006-C109006030030).

REFERENCE

[1] S. J. Wind, D. J. Frank, and H. –S. Wong, Microelectronic Engineering, 32 (1996) 271.

[2] D. Hisamoto et al. IEEE Trans. Electron Device, 47 (2000) 2320.

[3] L. Mathew, et al, VLSI Technology (2005) 200.

[4] M. Sabathil, S. Hackenbuchner, J. A. Majewski, G. Zandler, P. Vogl, J. Comp. Electronics. **1** (2002) 81.

[5] S. Lepaul, A. de Lustrac and F. Bouillault: IEEE Trans. Magn **32 (**1996) 1018.

[6] A. Svizhenko, M. P. Anantram, T. R. Govindan and B.Biegel, J. Appl. Phys. **91**, (2002) 2343.

[7] Kim K, Kwon O, Seo J, and T. Won, Journal of the Korean physical society 45 (2004) 1384.